

# Geophysical Research Letters®



## RESEARCH LETTER

10.1029/2024GL113316

## Climate Models Underestimate Global Decreases in High-Cloud Amount With Warming

S. Wilson Kemsley<sup>1</sup> , P. Nowack<sup>2,3</sup> , and P. Ceppi<sup>4</sup> 

<sup>1</sup>Climatic Research Unit, School of Environmental Sciences, University of East Anglia, Norwich, UK, <sup>2</sup>Institute of Theoretical Informatics, Karlsruhe Institute of Technology, Karlsruhe, Germany, <sup>3</sup>Institute of Meteorology and Climate Research (IMK-ASF), Karlsruhe Institute of Technology, Karlsruhe, Germany, <sup>4</sup>Department of Physics, Imperial College London, London, UK

### Key Points:

- Cloud-controlling factor analysis is applied for the first time to observationally constrain high-cloud amount feedback
- We find evidence for an observed stability iris mechanism that is misrepresented or missing in several climate models
- Observations suggest global decreases in high-cloud amount, resulting in near-neutral feedback from opposing longwave and shortwave changes

### Supporting Information:

Supporting Information may be found in the online version of this article.

### Correspondence to:

S. Wilson Kemsley,  
s.wilson-kemsley@uea.ac.uk

### Citation:

Wilson Kemsley, S., Nowack, P., & Ceppi, P. (2025). Climate models underestimate global decreases in high-cloud amount with warming. *Geophysical Research Letters*, 52, e2024GL113316. <https://doi.org/10.1029/2024GL113316>

Received 25 OCT 2024

Accepted 11 FEB 2025

### Author Contributions:

**Conceptualization:** S. Wilson Kemsley, P. Nowack, P. Ceppi

**Data curation:** S. Wilson Kemsley, P. Nowack, P. Ceppi

**Formal analysis:** S. Wilson Kemsley

**Funding acquisition:** P. Nowack, P. Ceppi

**Investigation:** S. Wilson Kemsley

**Methodology:** S. Wilson Kemsley, P. Nowack, P. Ceppi

**Supervision:** P. Nowack, P. Ceppi

**Validation:** S. Wilson Kemsley

**Visualization:** S. Wilson Kemsley

**Writing – original draft:** S. Wilson Kemsley

**Writing – review & editing:** S. Wilson Kemsley, P. Nowack, P. Ceppi

**Abstract** Cloud feedback has prevailed as a leading source of uncertainty in climate model projections under increasing atmospheric carbon dioxide. Cloud-controlling factor (CCF) analysis is an approach used to observationally constrain cloud feedback, and subsequently the climate sensitivity. Although high clouds contribute significantly toward uncertainty, they have received comparatively little attention in CCF and other observational analyses. Here we use CCF analysis for the first time to constrain the *high*-cloud radiative feedback, focusing on the cloud amount component owing to its dominant contribution to uncertainty in high-cloud feedback. Globally, observations indicate larger decreases in high cloudiness than state-of-the-art climate models suggest. In fact, half of the 16 models considered here predict radiative feedbacks inconsistent with observations, likely due to misrepresenting the stability iris mechanism. Despite the suggested strong high-cloud amount decreases with warming, observations point toward a near-neutral net high-cloud amount radiative feedback, owing to almost canceling longwave and shortwave contributions.

**Plain Language Summary** As the atmosphere warms, the structure and location of clouds within the atmosphere changes, which can exert an additional warming or cooling effect at the Earth's surface. Cloud-controlling factor analysis derives relationships between meteorological variables and clouds, in an attempt to reduce uncertainties in model estimates of this 'cloud feedback'. Within the CCF framework, low-level clouds have been widely studied but high clouds have received comparatively little research focus. Here, we find that the response of high clouds to warming in many climate models is not supported by observational evidence. For instance, many models predict widespread increases in the amount of high cloud under warming, while our observational evidence suggests reductions under global warming. Through understanding these changes, we show that we can in turn reduce the uncertainty in the feedback effect of high clouds on global warming.

## 1. Introduction

Clouds strongly modulate the global top-of-the-atmosphere (TOA) energy balance and are the largest source of uncertainty in the climate response to greenhouse gas forcing (Sherwood et al., 2020; Zelinka et al., 2022). A combination of model and observational evidence indicates that global cloud feedback is positive and thus amplifies global warming, though the magnitude of this effect remains uncertain (Ceppi & Nowack, 2021; Sherwood et al., 2020; Zelinka et al., 2020).

It is widely agreed that three large-scale mechanisms are the primary contributors toward cloud feedback (Ceppi et al., 2017): a reduction in tropical low-cloud amount (a positive shortwave effect), an increase in high-latitude low-cloud optical depth (a negative shortwave effect) and a rise in free-tropospheric cloud altitude (a positive longwave effect). It is also thought that changes in the amount and thickness of tropical anvil clouds contribute small but highly uncertain feedbacks (Bony et al., 2016; Sherwood et al., 2020; Zelinka et al., 2016).

Cloud-controlling factor (CCF) analysis is one approach used to constrain modeled cloud feedback (Ceppi & Nowack, 2021; Myers et al., 2021; Nowack & Watson-Parris, 2024; Qu et al., 2015). Understanding and constraining the response of low—more specifically, tropical marine—clouds to global warming has consistently been a prominent research focus within the cloud feedback community (Ceppi et al., 2024; Myers et al., 2021; Myers & Norris, 2016; Qu et al., 2014, 2015; Scott et al., 2020; Wyant et al., 2009), motivated by their large contributions to the inter-model variance in climate projections (Sherwood et al., 2014; Webb et al., 2013).

© 2025. The Author(s).

This is an open access article under the terms of the [Creative Commons Attribution License](https://creativecommons.org/licenses/by/4.0/), which permits use, distribution and reproduction in any medium, provided the original work is properly cited.

Consequently, meteorological controls for low clouds are now comparatively well understood (Andersen et al., 2022, 2023; Fuchs et al., 2018; Klein et al., 2017).

High clouds have been less emphasized in CCF analyses and observational constraints, despite their significant contributions toward cloud feedback uncertainty (Raghuraman et al., 2024; Sherwood et al., 2020; Williams & Pierrehumbert, 2017). The physics governing the rise of free-tropospheric cloud altitude with global warming is well understood and supported by observational studies (Hartmann & Larson, 2002; Sherwood et al., 2020; Zelinka & Hartmann, 2010). As the atmosphere warms, the altitude range where significant radiative water vapor cooling occurs expands upwards. Longwave emission by free-tropospheric clouds therefore occurs at a higher altitude and colder temperature, resulting in a positive cloud feedback. This simple mechanism is relatively well captured by modern climate models, subsequently resulting in a small uncertainty range compared to other contributions to the overall cloud feedback (Sherwood et al., 2020).

Expert assessments such as the World Climate Research Program (WCRP) also estimate a highly uncertain, but possibly stabilizing, tropical anvil cloud area feedback (Sherwood et al., 2020), motivated by theory and observational evidence (Saint-Lu et al., 2020, 2022; Williams & Pierrehumbert, 2017). The “stability iris theory” states that as the atmosphere warms, static stability also increases, consequently decreasing horizontal convergence and reducing anvil cloud outflow from deep convection (Bony et al., 2016). Similarly, as high clouds rise, they find themselves in a more stable atmosphere due to the inverse relationship between static stability and atmospheric pressure (Zelinka & Hartmann, 2010, 2011) which, in turn, also reduces convective outflow (Bony et al., 2016). Many observational studies—typically based on inter-annual variability—support a reduction in tropical high-cloud amount with warming, though the net radiative effect is uncertain due to compensating longwave (LW) and shortwave (SW) feedbacks (Bony et al., 2016; Williams and Pierrehumbert, 2017; Saint-Lu et al., 2020; Beydoun et al., 2021).

In this article, we build upon the work of Wilson Kemsley et al. (2024, hereafter WK24) and Ceppi and Nowack (2021, hereafter CN21) to constrain the radiative feedback due to changes in the amount of high cloud using CCF analysis for the first time. CN21 built upon traditional CCF analyses by using ridge regression instead of multiple linear regression (MLR). This allowed CCFs within large spatial domains to be considered, motivated by the understanding that the life-cycle of clouds occurs over synoptic scales. CN21 showed that larger spatial domains resulted in improved feedback prediction skill compared to traditional MLR approaches using local CCFs. To address the lack of high-cloud specific analyses, WK24 systematically reviewed a selection of controlling factors targeting the life-cycle of *high* clouds and their theorized feedback mechanisms. WK24's work highlighted static stability in the upper troposphere ( $S_{UT}$ ) and a measure of wind shear between the surface and 300 hPa ( $\Delta U_{300}$ ) as new candidate CCFs for high-cloud feedback constraints. Here we utilize CN21's approach with WK24's cloud-controlling factors—surface temperature ( $T_{sfc}$ ), relative humidity at 700 hPa ( $RH_{700}$ ), upper tropospheric relative humidity (UTRH), vertical velocity at 300 hPa ( $\omega_{300}$ ),  $S_{UT}$  and  $\Delta U_{300}$ —to constrain the high-cloud amount feedback.

## 2. Data and Methodology

### 2.1. Data Sets

This research uses monthly mean meteorological and cloud data, re-gridded to a  $5^\circ \times 5^\circ$  resolution. For observed cloud-radiative anomalies, we use 21 years (July 2002 to June 2023) of data from the combined Moderate Resolution Imaging Spectroradiometer (MODIS) retrievals from the Aqua and Terra instruments (identified as MCD06COSP; Pincus et al., 2023). We use only MODIS; we found artifacts and missing data in cloud-radiative histograms from other observational data sets had a substantial impact on the estimated relationships (not shown, see Norris & Evan, 2015). As a proxy for direct observations, we use ERA5 CCFs (for the calculation of the CCFs, see Text S1 in Supporting Information S1). To sample observational uncertainty, we use a bootstrapping approach detailed in Section 2.3.

For climate model validation, we use historical and abrupt-4xCO<sub>2</sub> cloud fraction histograms and CCFs from 16 general circulation models (GCMs) from Coupled Model Intercomparison Project phases 5 and 6 (CMIP5/6) experiments that have run the International Satellite Cloud Climatology Project (ISCCP) simulator. We restrict the time period to 20 years, aligning with the length of our bootstrapped observational data sets. For the models, we use January 1981 to December 2000 because it is close to the present-day climate and within the availability of

*historical* simulations. For abrupt-4xCO<sub>2</sub> CCF responses, we use an additional 34 climate models, totaling 50. For both models and observations, we only consider grid-cells with latitudes centered between 60°S–60°N due to poor cloud amount retrievals at low sun angles, and therefore references to “global” averages are calculated within this range, with values scaled with respect to the fraction of global area considered (multiplied by 0.86).

## 2.2. Radiative Anomalies

Cloud-radiative kernels are used to partition cloud-radiative anomalies,  $R$ , into contributions from changes in cloud amount (AMT), cloud top pressure and optical depth, with the same kernels for observed and modeled  $R$  (Zelinka et al., 2012a, 2012b). We isolate  $R$  from non-low clouds (hereafter “high clouds” for conciseness) according to their cloud top pressures. For MODIS, we follow previous studies (e.g., Zelinka et al., 2016) and retain top pressures <680 hPa. For CMIP ISCCP simulator data, we use a lower cutoff pressure of 560 hPa. This is because the ISCCP simulator tends to misattribute mid-level clouds in the 560–680 hPa range to higher pressure levels (Ceppi et al., 2024). All references to cloud-radiative anomalies and feedback henceforth are for high clouds unless made explicit otherwise. Similar to other CCF analyses, we remove the seasonal cycles from the CCFs and radiative anomalies (Andersen et al., 2022; Myers et al., 2021; Wilson Kemsley et al., 2024). The cloud-radiative kernel method relies on properties derived from passive satellite sensors (in the case of observations) or simulators (for the CMIP models). As such, changes in obscuration of low-level clouds by upper-level clouds impacts the partitioned cloud feedbacks, which we account for here (Zelinka et al., 2024).

## 2.3. Statistical Learning Framework

Observationally constraining cloud feedback is a multi-step process. We first use ridge regression to learn the *historical* sensitivities,  $\Theta$ , to six CCFs ( $T_{\text{sfc}}$ , RH<sub>700</sub>, UTRH,  $\omega_{300}$ ,  $S_{\text{UT}}$  and  $\Delta U_{300}$ ) at each grid-cell  $r$ . For each regression, we consider factors within a spatial domain centered on  $r$  corresponding to 105° × 55° (21 longitude × 11 latitude points). These grid-cell specific regressions are carried out independently for each of the 16 GCMs. Our choice of domain size and statistical learning method is further discussed in Texts S2–S4 in Supporting Information S1.

We subsequently predict the cloud-radiative responses under abrupt-4xCO<sub>2</sub> forcing and normalize these by the modeled simultaneous global mean surface temperature (GMST) increase to obtain radiative feedback units. This is done individually for each GCM at each grid-cell using historical sensitivities multiplied by the model-consistent CCF responses per unit GMST increase;

$$\frac{dR(r)}{dT} \approx \sum_{i=1}^M \Theta_i \frac{dX_i(r)}{dT}, \quad (1)$$

where  $\Theta_i$  is the sensitivity of  $R(r)$  to the  $i$ -th CCF ( $X_i$ ) and  $M$  is the number of model dimensions ( $M = 1386$ ). Note that  $X$  and  $\Theta$  are spatial maps, where  $i$  is the  $i$ -th grid-cell within the 21 × 11 spatial domain centered on  $r$ .

We use all six CCFs in the extrapolation (Text S1 in Supporting Information S1). To estimate the global high-cloud feedback parameter, we take the spatially weighted global mean of the local regressions,  $\frac{dR(r)}{dT}$ , which we refer to as the “CMIP predicted” feedback. We subsequently determine the prediction error between the global-mean “CMIP actual” feedback (i.e., determined using Gregory regressions from abrupt-4xCO<sub>2</sub> simulations; Gregory et al., 2004) and the “CMIP predicted” feedback (Ceppi & Nowack, 2021; Nowack et al., 2023).

To obtain an observational constraint on the modeled cloud feedback terms, we use the  $\Theta_i$  estimated from 20-year of MODIS data. To sample observational uncertainty, we bootstrap (with replacement) the original MODIS (and ERA5) data sets to produce 10 20-year long data sets. This results in 10 observational estimates for the cloud-radiative sensitivities at each grid-point. We then multiply observed sensitivities with the GCM CCF responses to warming ( $dX_i(r)/dT$  in Equation 1), substituting our observed estimates for  $\Theta_i$  and using the 50 CMIP abrupt-4xCO<sub>2</sub> CCF responses. Finally, to constrain cloud feedback, we convolve the resulting probability density function with the prediction error from the CMIP validation. For details about this process, see Text S4 (Ceppi & Nowack, 2021; Nowack et al., 2023).

Throughout this article, radiative anomalies,  $R$ , and *global* cloud feedback,  $\lambda$ , are referred to using subscripts. Cloud radiative anomalies induced by changes in cloud amount are referred to using an additional subscript, for example,  $\lambda_{LW,AMT}$  is the LW feedback from changes in high-cloud amount with all other properties held fixed.

### 3. Results

We apply our framework to predict  $\lambda_{LW,AMT}$  and  $\lambda_{SW,AMT}$  separately. Negative  $\lambda_{LW,AMT}$  would arise from global decreases in cloud amount due to reduced absorption of upwelling LW radiation. This accordingly corresponds to *positive*  $\lambda_{SW,AMT}$  due to reduced reflection of incident SW radiation. Our best estimates of  $-0.29 \text{ W m}^{-2} \text{ K}^{-1}$  and  $0.22 \text{ W m}^{-2} \text{ K}^{-1}$  (Figures 1b and 1d) for  $\lambda_{LW,AMT}$  and  $\lambda_{SW,AMT}$ , respectively, are similar in magnitude with opposing direction (Table S1 in Supporting Information S1). Observationally constrained ranges are now robustly (90% confidence) negative (LW) and positive (SW), posing a stark contrast to the CMIP model estimates which are more equally distributed into negative and positive feedback terms for both SW and LW (shown in Figures 1b and 1d). Thus, our constraint supports the suggested mechanism of high-cloud amount reductions and the associated impacts on the LW and SW radiative bands, in contrast to models that simulate a range of high-cloud amount responses.

Though our focus is on the radiative feedbacks, we repeat our analysis to constrain global high-cloud amount (AMT, expressed as a percentage of total grid-box area) changes with warming ( $\frac{dAMT}{dT}$ ). Climate models predict a range of responses, with a neutral mean (note that the units  $\% \text{ K}^{-1}$  are absolute percentage points rather than fractional changes). Our constrained best estimate is negative ( $-0.18\% \text{ K}^{-1}$ ), with less than 20% chance of global increases. This indicates that GCMs underestimate global reductions in high-cloudiness with warming (Figure 1f). Thus, our negative estimate for  $\frac{dAMT}{dT}$  is consistent with negative  $\lambda_{LW,AMT}$  and positive  $\lambda_{SW,AMT}$ . While our constrained  $\frac{dAMT}{dT}$  is more negative than the model mean, the difference is less pronounced than the feedback components. Therefore, though it is evident that climate models underestimate decreases in high-cloudiness, they also tend to underestimate the associated radiative impacts.

The observationally constrained negative  $\lambda_{LW,AMT}$  and positive  $\lambda_{SW,AMT}$  have implications on respective high-cloud feedbacks from all cloud properties. The multi-model mean  $\lambda_{LW}$  and  $\lambda_{SW}$  are positive and negative, respectively (though with considerable inter-model uncertainty regarding sign; Figure S2 in Supporting Information S1). Observations instead indicate a lower (near-neutral) central estimate for  $\lambda_{LW}$  and a *positive* central estimate for  $\lambda_{SW}$ . Our observational best estimates are consistent with CN21, who found their constrained central estimates for LW feedback from *all* clouds are less positive than the climate model mean (and conversely for SW). We find that the much stronger radiative feedback associated with the greater reduction of high-cloudiness in the observations is at least partially responsible for this discrepancy (Ceppi & Nowack, 2021, their Figure S3 in Supporting Information S1).

Reductions in high-cloud amount over the West Pacific and Maritime Continent, alongside increases in the East Pacific, are present in observations and the multi-model mean (Figure 2 and Figure S9 in Supporting Information S1). Local magnitudes for  $\frac{dR_{AMT}}{dT}$  and  $\frac{dAMT}{dT}$  are ubiquitously larger in the observations than in the model average, indicating consistently stronger changes in areal coverage and associated radiative forcing at local scales as well as globally. Therefore, despite relatively similar global  $\lambda_{NET,AMT}$  (see below), local impacts and effects on the circulation may differ. For example, there is GCM evidence that the areal coverage of high clouds may modulate changes in the El Niño–Southern Oscillation (Nowack et al., 2015, 2017; Rädel et al., 2016).

Convolving our observationally constrained  $\lambda_{LW,AMT}$  and  $\lambda_{SW,AMT}$  distributions yields an approximately neutral estimate for  $\lambda_{NET,AMT}$  of  $-0.04 \text{ W m}^{-2} \text{ K}^{-1}$  (Bretherton & Caldwell, 2020, see Text S5 in Supporting Information S1). The multi-model mean  $\lambda_{NET,AMT}$  is within the 66% confidence range of observational uncertainty (Figure 2h), though many climate models predict positive  $\lambda_{LW,AMT}$  and/or negative  $\lambda_{SW,AMT}$ , aligning with global *increases* in high-cloud amount (Figure 1f). Such feedbacks are highly improbable based on our constraint—in fact, positive  $\lambda_{LW,AMT}$  is less than 5% likely based on our evidence, despite being positive in half of the climate models. Instead, GCMs with  $\lambda_{LW,AMT}$  and  $\lambda_{SW,AMT}$  toward the lower and upper tail ends (respectively) of the climate model distribution are more aligned with our observational estimate.

Our value for  $\lambda_{NET,AMT}$  is closer to more neutral estimates for high-cloud amount feedbacks derived from regional observational analyses and theory than the WCRP's central estimate of  $-0.20 \text{ W m}^{-2} \text{ K}^{-1}$ . For example, our

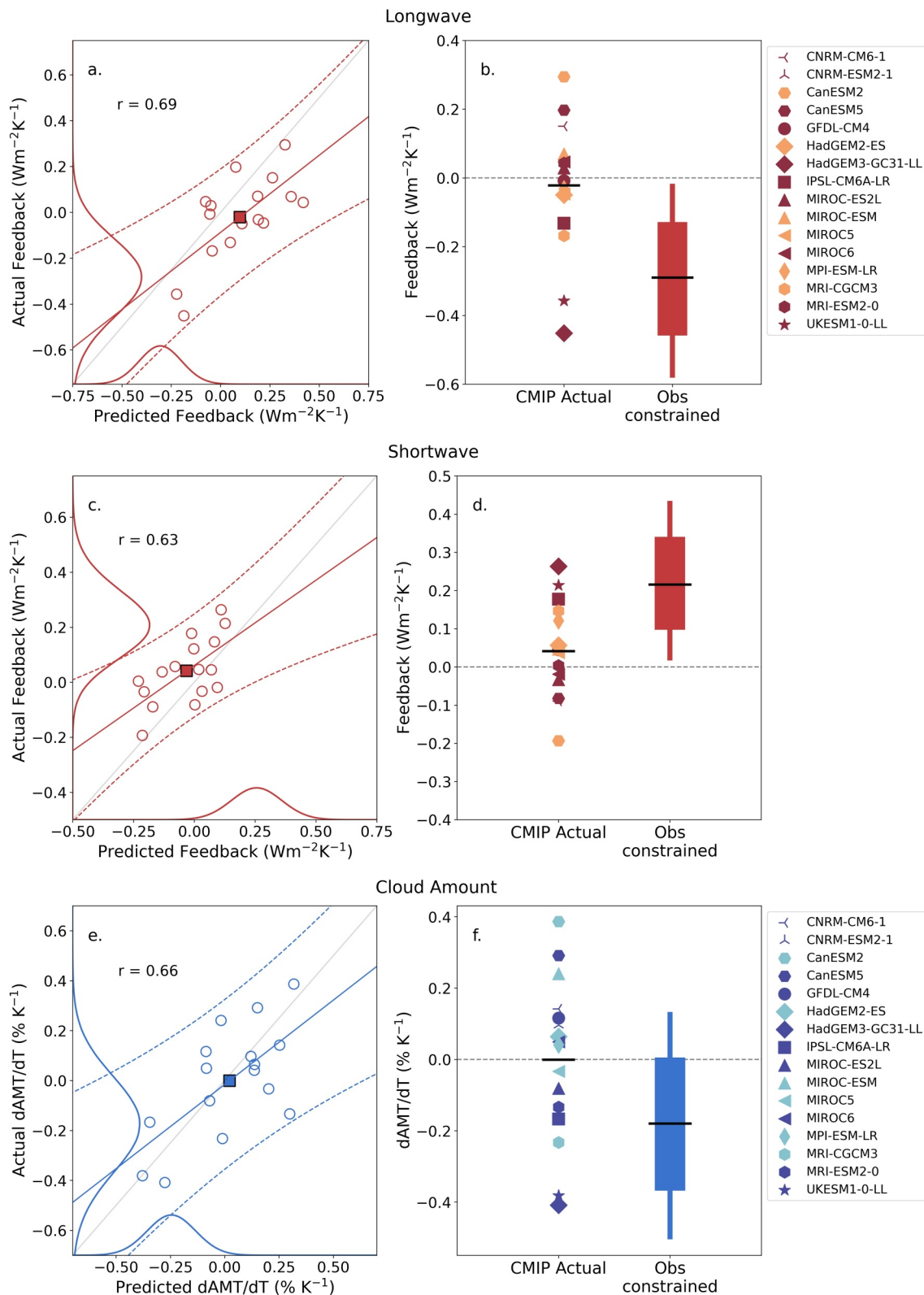


Figure 1.

estimate of  $-0.04 \text{ W m}^{-2} \text{ K}^{-1}$  lies close to Raghuraman et al. (2024)'s estimate of  $-0.03 \text{ W m}^{-2} \text{ K}^{-1}$  and McKim et al. (2024)'s estimate of  $0.02 \text{ W m}^{-2} \text{ K}^{-1}$  (note these are specifically for *anvil* cloud). We also derive a smaller uncertainty of  $\sigma = 0.065 \text{ W m}^{-2} \text{ K}^{-1}$ , compared with the WCRP's  $\sigma = 0.20 \text{ W m}^{-2} \text{ K}^{-1}$ . Note that our method for constraining  $\lambda_{\text{NET,AMT}}$  is somewhat sensitive to the underlying GCM distribution, which has smaller  $\sigma$  than the WCRP feedback (CMIP  $\sigma = 0.08 \text{ W m}^{-2} \text{ K}^{-1}$ ). Regardless, our constrained estimate corresponds to approximately a 20% reduction in the CMIP standard deviation.

The observed spatial distribution shown in Figure 2e suggests that reduced cloudiness in the deep tropics—where anvil clouds are abundant—contributes negatively toward  $\lambda_{\text{NET,AMT}}$ ; though this is more poorly agreed upon across our 10 realizations than for the LW and SW components (hatching in Figure 2e). Based on observational estimates of short-term cloud feedback, Williams and Pierrehumbert (2017) found that SW feedback is less effective at canceling out LW in deep convective regimes, possibly resulting in the negative regions shown in Figure 2e. This does not imply a negative global feedback, however, as high clouds do not only exist in deep convective regimes. Accounting for tropical high clouds outside of deep convective regimes, Raghuraman et al. (2024) show that positive feedback from non-deep convective high clouds approximately balances deep convective negative amount feedback. Given that our estimate for  $\lambda_{\text{NET,AMT}}$  is near-neutral, negative contributions toward  $\lambda_{\text{NET,AMT}}$  from reductions in tropical anvil cloud amount appear too weak to drive a global negative feedback, highlighting the sensitivity of high-cloud amount feedback estimates to spatial sampling (Raghuraman et al., 2024).

### 3.1. Exploring the Role of Thick and Thin Clouds

We evaluate high-cloud amount feedback driven by thin and thick clouds by summing  $R$  over optical depth bins with  $\tau \leq 4.5$  and  $\tau > 4.5$ , respectively, before regressing against GMST. For discussion purposes, we approximate thick high clouds as highly reflective deep convective cores with relatively low abundance but strong radiative impacts (Chen et al., 2000), and thin clouds to detrained anvil and in-situ cirrus (Gasparini et al., 2023). Figure 3 shows thin and thick-cloud amount feedbacks are constrained well by our framework given their tight confidence ranges, which is most striking for thin clouds. We also find that both thick and thin cloud amount feedbacks are robustly negative for LW and positive for SW (90% confidence), which is again in contrast with the uncertain direction of the CMIP predicted feedbacks.

A robust decrease in thick cloud amount with warming has been speculated by previous studies (e.g., Sokol et al., 2024), which we find strong evidence for (Figure 3, “Thick”). This may be due to reductions in amount *or* decreased optical depth, which would shift summations from “thick” to “thin” bins. Our best estimates for the LW and SW components are approximately equal in magnitude though with opposing signs, indicating a radiatively neutral feedback emanating from changes in the amount of thick cloud. Increased convective organization, reductions in the number of convective events and decreases in typical anvil areal extent would all manifest in reduced deep convective and fresh anvil cloud amount (Sokol et al., 2024; Wodzicki & Rapp, 2022).

Previous evidence is more inconclusive regarding changes to thin-cloud amount (Sokol et al., 2024). We find compelling evidence for reductions in the amount of such clouds. Our constrained thin-cloud amount feedbacks are smaller in magnitude ( $-0.11$  and  $0.06 \text{ W m}^{-2} \text{ K}^{-1}$  for LW and SW, respectively) than their thick counterparts, but less balanced. Compared to thicker clouds, radiative effects from optically thin cirrus are typically not as large but imbalances between the SW and LW components can make them more important for net cloud feedback (McFarquhar et al., 2000). Thin-cloud amount feedbacks are governed by the interplay between opposing decreases in thin cloud amount and *increases* in thin cloud due to thinning of thick cloud. A reduction in thin cloud amount may be caused by increases in static stability, thus suppressing horizontal detrainment (Bony et al., 2016; Saint-Lu et al., 2020, 2022). In contrast, recent evidence suggests that a thinning of thick cloud is likely as the

**Figure 1.** Panels (a) and (c) show actual versus predicted global-mean LW ( $\lambda_{\text{LW,AMT}}$ ) and SW ( $\lambda_{\text{SW,AMT}}$ ) high-cloud feedback, respectively, for 16 CMIP models (empty circles) and the multi-model mean (filled square). Panel (e) similarly shows the high-cloud amount change per degree global mean surface temperature (GMST) increase ( $\frac{d\text{AMT}}{dT}$ ). The solid colored lines are the least squares fits, and colored dashed lines the 5%–95% prediction intervals. Colored curves are the probability distributions for observational estimates, with amplitudes arbitrarily scaled. Panels (b), (d) and (f) show CMIP model global  $\lambda_{\text{LW,AMT}}$ ,  $\lambda_{\text{SW,AMT}}$ , and  $\frac{d\text{AMT}}{dT}$  respectively, and observational constraints (denoted “Obs constrained”). CMIP5 and CMIP6 models are denoted using light and dark symbols, respectively. Thin and thick bars in (b), (d), and (f) Denote the 90 and 66% confidence intervals, respectively. Black horizontal bars correspond to the mean CMIP feedbacks and the median (50th percentile) for the observational constraints. Values have been scaled by the global area weighting (0.86).

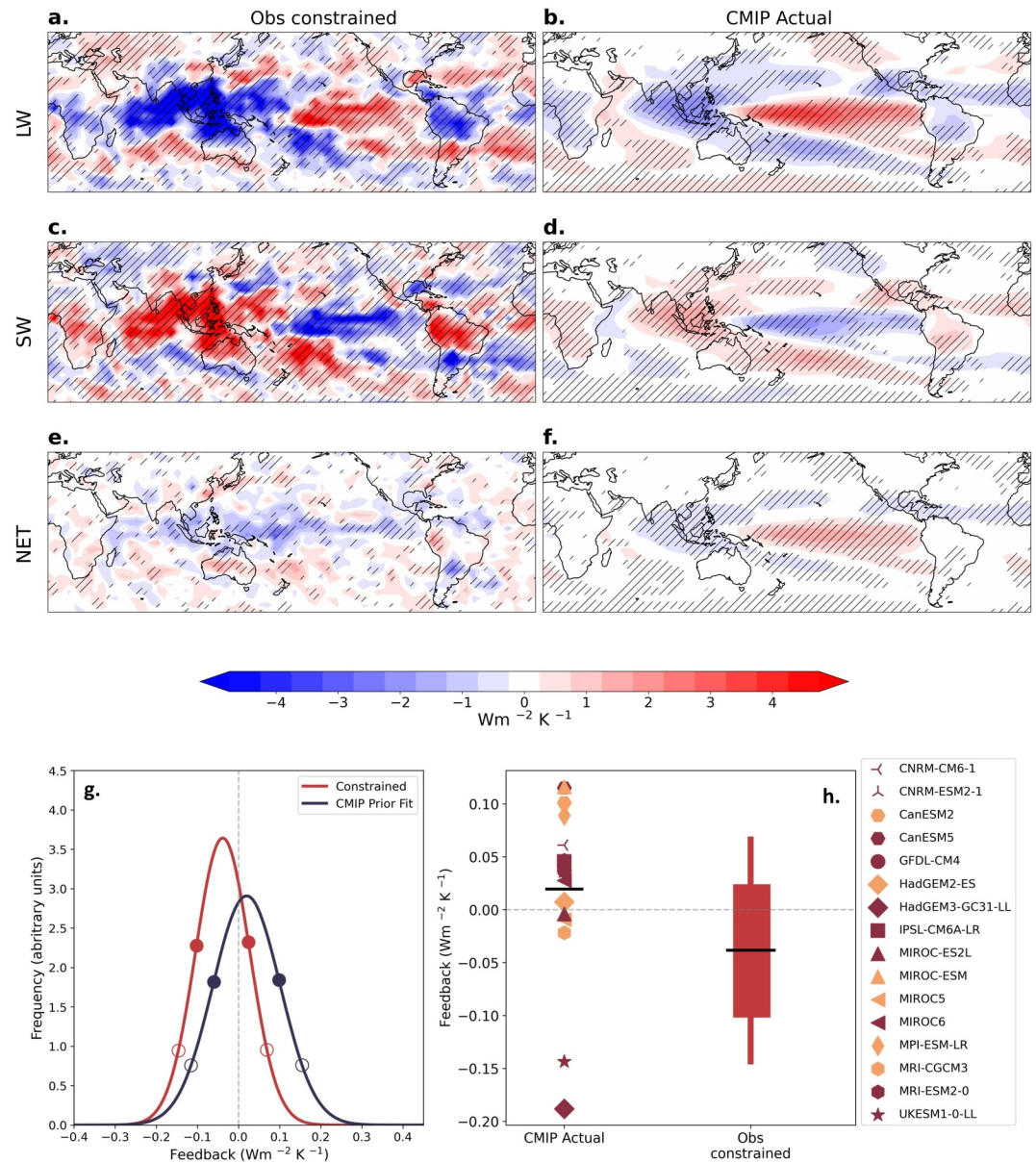


**Figure 2.** Observationally constrained and CMIP “Actual” high-cloud amount feedback for (a–b) longwave (LW), (c–d) shortwave (SW), and (e–f) net (LW + SW) feedback ( $\lambda_{\text{NET,AMT}}$ ). Observed cloud feedback is obtained using the mean MODIS sensitivities ( $N_{\text{MODIS}} = 10$ ) multiplied by the mean CMIP CCF abrupt-4xCO<sub>2</sub> responses ( $N_{\text{CMIP}} = 50$ ). Hatching denotes regions where at least 80% of the local cloud radiative responses have the same sign; for the left column, this is  $\geq 8$  of the mean observational realizations and the right column,  $\geq 13$  climate models. Panel (g) shows distributions for  $\lambda_{\text{NET,AMT}}$  in the CMIP models (CMIP Prior Fit) and our constrained distribution. The central best estimate for the constrained distribution is  $-0.04 \text{ W m}^{-2} \text{ K}^{-1}$  and for the CMIP Prior,  $0.02 \text{ W m}^{-2} \text{ K}^{-1}$ . Panel (h) shows the CMIP actual  $\lambda_{\text{NET,AMT}}$  with the multi-model-mean denoted by a solid black bar and the corresponding observational constraint (“Obs constrained”), with the same corresponding confidence ranges as Figures 1b–1d and 1f. Values in (g–h) have been scaled by the global area weighting (0.86).

atmosphere warms (Raghuraman et al., 2024; Sokol et al., 2024), which would subsequently increase the ratio of thin to thick clouds and exert an optical depth feedback.

### 3.2. Sensitivities to the Cloud-Controlling Factors

An advantage of CCF analysis is its interpretable regression coefficients. We use the CCF sensitivities to investigate whether mechanistic differences between models and observations explain the differences in high-

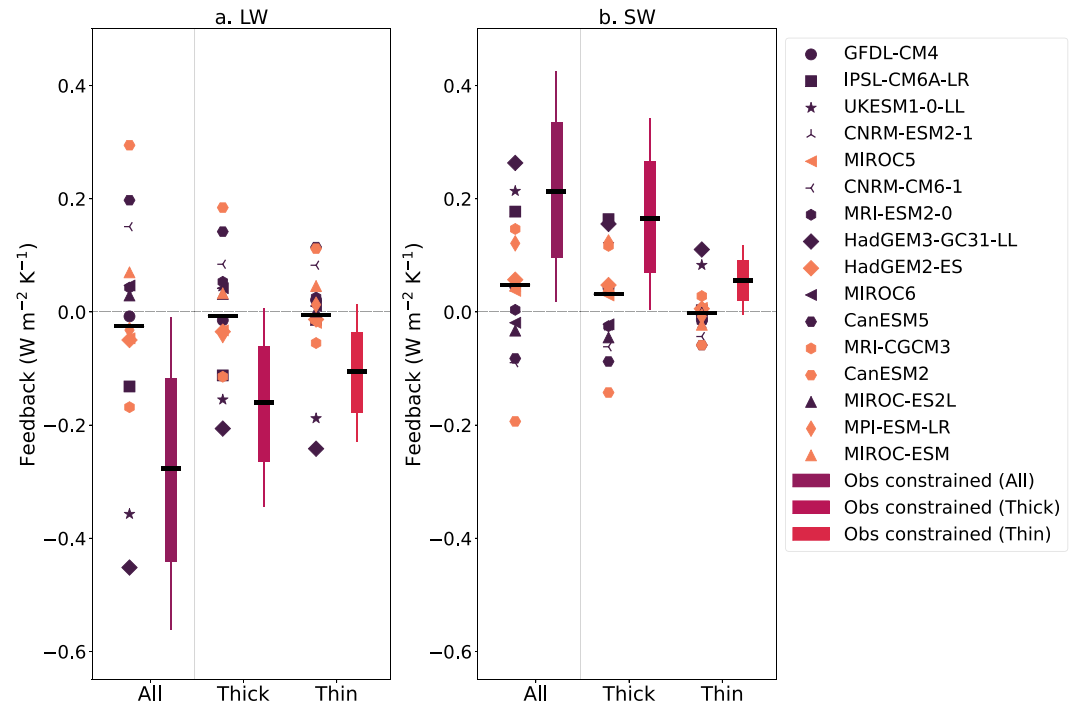


**Figure 3.** CMIP global-mean high-cloud feedback partitioned into changes from cloud amount only, and corresponding observational constraints (“Obs constrained”) for (a) Longwave (LW) and (b) shortwave (SW). Values have been scaled by the global area weighting (0.86). Thin and thick bars denote the 90 and 66% confidence intervals, respectively. Black horizontal bars show the mean CMIP actual feedback and observational best estimate (50th percentile). Thick and thin cloud amount feedback is also shown, summed over optical depths  $>4.5$  and  $\leq 4.5$  respectively (see text). The central estimates for the LW high-cloud amount feedback summed over all, thick, and thin optical depth bins are  $-0.29$ ,  $-0.16$ , and  $-0.11$   $\text{W m}^{-2} \text{K}^{-1}$ , respectively. Similarly for SW the central estimates for all, thick and thin clouds are  $0.22$ ,  $0.17$ , and  $0.06$   $\text{W m}^{-2} \text{K}^{-1}$ , respectively. The climatological global mean percentage of thick and thin high cloud for the models and observations can be found in Figure S8 in Supporting Information S1. Values for further percentiles can be found in Table S1 in Supporting Information S1.

cloud amount reduction. Here, we focus on the CCFs with the largest contributions toward both the magnitude and uncertainties in global mean high-cloud amount feedback:  $T_{\text{sfc}}$  and  $S_{\text{UT}}$  (Figure S7 in Supporting Information S1). The sensitivities for the additional CCFs are shown in Figures S4–S5 in Supporting Information S1.

The sensitivity of cloud amount to thermodynamic controls—specifically  $T_{\text{sfc}}$  and  $S_{\text{UT}}$ —appears to play a major role in the inter-model uncertainty. The  $T_{\text{sfc}}$  sensitivities in the Maritime Continent and Western Pacific are poorly agreed upon by the GCMs (hatching in Figures 4c and 4g and Figure S10 in Supporting Information S1), resulting in a weak multi-model mean sensitivity in these regions. Subsequently, the  $T_{\text{sfc}}$  contributions toward  $\lambda_{\text{LW,AMT}}$  and  $\lambda_{\text{SW,AMT}}$  are highly variable and contrast the observed influence of  $T_{\text{sfc}}$  on the feedback (Figure S7 in Supporting Information S1). Historical climate model sea surface temperature (SST) warming patterns have shown significant mismatches to observations (Wills et al., 2022). To discern whether differences in spatial sensitivities between models and observations result from different SST patterns, we re-calculate the sensitivities using Atmospheric Model Intercomparison Project (AMIP) simulations (See Text S6 in Supporting Information S1). The discrepancy between climate model and observed  $T_{\text{sfc}}$  sensitivities remains in the AMIP simulations (Figure S10 in Supporting Information S1), and hence we attribute the differences to an underestimated stability iris mechanism in the climate models.

In the context of the stability iris, we would expect a reduction in anvil cloud coverage with increasing surface temperature in the deep convective tropics (Bony et al., 2016). Anvil clouds rise near-isothermally with  $T_{\text{sfc}}$ , finding themselves in a more stable environment (Zelinka & Hartmann, 2010, 2011). Accordingly, horizontal convergence is reduced which in turn reduces anvil cloud outflow (Bony et al., 2016; Saint-Lu et al., 2020, 2022; Wilson Kemsley et al., 2024) and subsequently the areal coverage. This would result in negative  $R_{\text{LW,AMT}}$



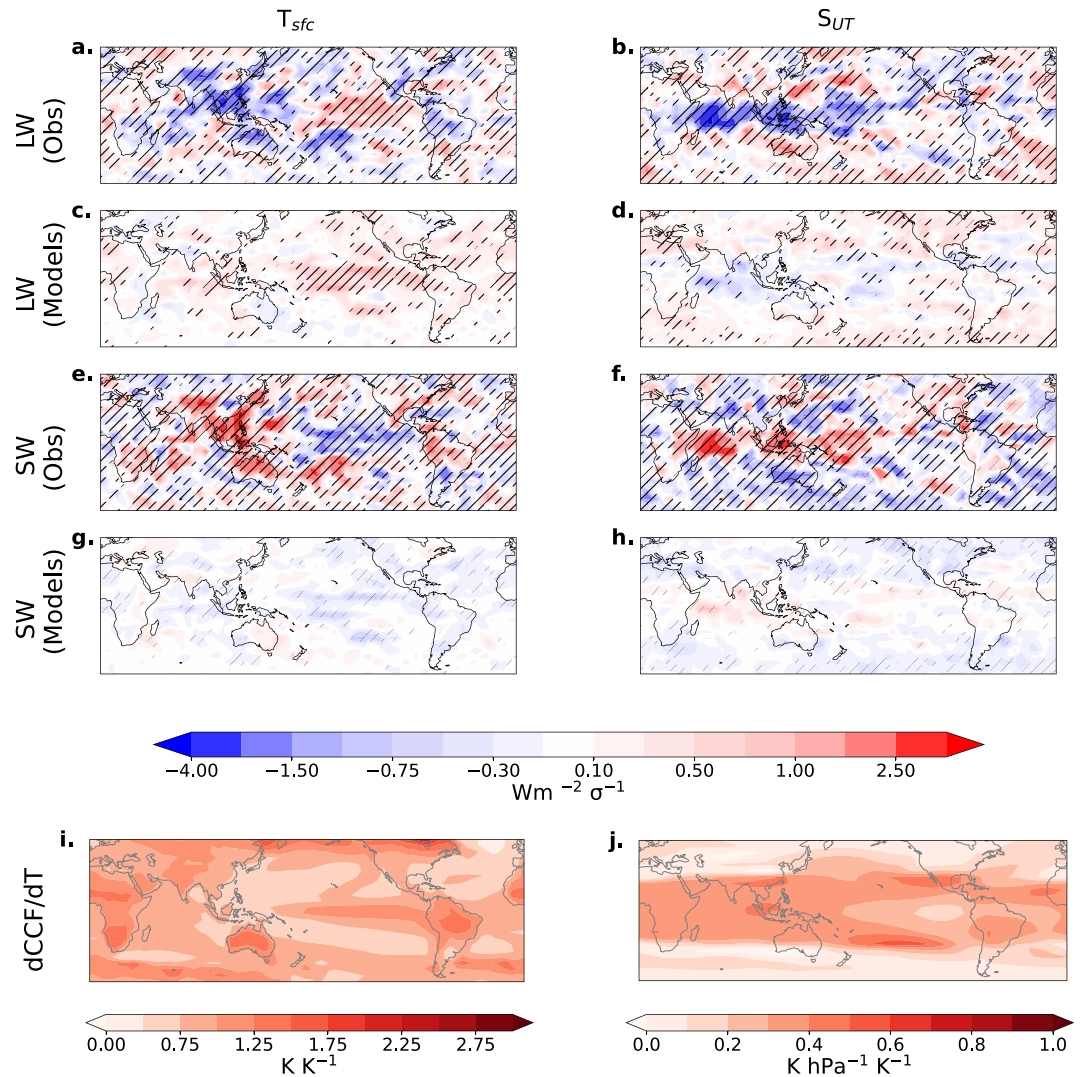


**Figure 4.** Panels (a–h) show the historically derived cloud-amount sensitivities to surface temperature,  $T_{sfc}$ , and upper-tropospheric static stability,  $S_{UT}$ , for  $R_{LW,AMT}$  and  $R_{SW,AMT}$ , in observations (“Obs”) and climate models (“Models”) - scaled by the ERA5 cloud-controlling factor standard deviations). To produce the maps, all elements of the sensitivity vectors are summed at each grid-point  $r$ . For observations, the mean across the 10 bootstrapped data sets is shown, and for models the multi-model mean is shown. Hatching denotes regions where  $\geq 8$  and  $\geq 13$  observed and modeled sensitivities, respectively, share the same sign. Panels (i–j) show the multi-model mean CCF responses,  $dX/dT$ , derived through linearly regressing the 50 abrupt-4xCO<sub>2</sub> responses against their corresponding global-mean surface temperature increases.

(positive  $R_{SW,AMT}$ ) sensitivities to  $T_{sfc}$ , which holds true for the observations but less so for the climate models (Figure S10 in Supporting Information S1). Inspection of the sensitivities in deep convective regions reveals *positive* LW (negative SW) sensitivities to  $T_{sfc}$  in several climate models (e.g., MIROC-ESM, MRI-ESM2-0, and CanESM2; Figure S6 in Supporting Information S1) or weak sensitivities in others. We speculate that the weak climate model  $T_{sfc}$  sensitivities are a trade-off between increased convection or vertical mixing with warmer SSTs—resulting in more cloud—versus the reduction in convective outflow and anvil cloud following stability iris physics.

As expected in a warming atmosphere,  $S_{UT}$  near-ubiquitously increases with GMST (Figure 4j). This increase is enhanced over the Western Pacific and Maritime Continent, collocating with the regions of strongest negative LW (and positive SW) observed sensitivity. This is reiterated by sizable negative (positive) contributions of  $S_{UT}$  toward the observationally constrained  $\lambda_{LW,AMT}$  ( $\lambda_{SW,AMT}$ ) shown in Figure S7 in Supporting Information S1. Observed  $S_{UT}$  sensitivities resemble the stability iris mechanism, where increased static stability drives reductions

in high-cloudiness due to reduced convective outflow from decreasing horizontal convergence (Bony et al., 2016; Saint-Lu et al., 2020, 2022). The climate models instead predict a smaller feedback driven by  $dS_{UT}/dT$  (Figure S7 in Supporting Information S1) due to weak sensitivities. For example, the multi-model mean  $R_{LW,AMT}$  sensitivity to  $S_{UT}$  in the Western Pacific is only slightly negative as a result of poor agreement between the models (Figures 4d–4h and Figure S10 in Supporting Information S1). Only half of the models have  $S_{UT}$  sensitivities similar in magnitude to the observations, and in many cases, the sensitivity is a different sign. This supports our reasoning that several climate models underestimate the stability iris mechanism and associated reductions in high-cloud amount.

The climate model UTRH sensitivities are well agreed upon, but despite strong magnitudes for the sensitivities (Figures S4, S5 in Supporting Information S1, and also WK24), UTRH has a smaller contribution toward the observationally constrained  $\lambda_{LW,AMT}$  and  $\lambda_{SW,AMT}$  than in the climate models. Though  $RH_{700}$ ,  $\omega_{300}$  and  $\Delta U_{300}$  sensitivities are typically large in magnitude (Figures S4 and S5 in Supporting Information S1) and important for historical predictions (WK24), their *global* contributions toward feedback are relatively small. However, their inclusions as CCFs improve local correlations between “actual” and “predicted” CMIP feedback, and are therefore important at local scales (not shown). Their globally averaged neutral contributions are largely due to cancellation from regions of opposing positives and negatives (Figure S3 in Supporting Information S1). Our findings align with previous research, wherein circulation changes (mainly captured by  $\omega_{300}$  and  $\Delta U_{300}$ ) are important regionally, but thermodynamic changes—related to  $T_{sfc}$  and  $S_{UT}$ —drive larger-scale cloud feedbacks (Bony et al., 2004; Byrne & Schneider, 2018).

#### 4. Discussion

Our observational evidence indicates that climate models underestimate global reductions in high-cloud amount and associated LW and SW radiative feedbacks with warming. We mainly ascribe this to different sensitivities within the climate models for  $T_{sfc}$  and  $S_{UT}$ . Previous studies suggest that climate models underestimate the anvil cloud feedback compared to expert assessments due to the poor representation of convective organization processes and cloud microphysics (Sherwood et al., 2020; Zelinka et al., 2022). We also attribute climate models' smaller reductions in high-cloud amount partly to their underestimation of the stability iris mechanism. For example, in the Western Pacific and Maritime Continent, the observed sensitivities to  $T_{sfc}$  and  $S_{UT}$  are *both* negative for  $R_{LW,AMT}$  (and positive for  $R_{SW,AMT}$ ), collocating with the regions of most abundant high cloud (Figures S8, S10 in Supporting Information S1). However, in these regions, the climate model  $T_{sfc}$  sensitivities are typically the wrong sign relative to observations, and the multi-model mean  $S_{UT}$  sensitivity is weak due to poor agreement within the GCMs. This indicates that the physical mechanisms of high-cloud feedback present in the observations are not being adequately captured by many of these climate models.

Our near-neutral best estimate for  $\lambda_{NET,AMT}$  does not indicate a stabilizing high-cloud amount feedback and is close to the multi-model mean  $\lambda_{NET,AMT}$  (despite GCMs being “right” for the “wrong” reasons in several cases). Though Figure 2 provides evidence for negative feedback in deep convective regions, globally this is balanced by regions of positive feedback. Our evidence thus indicates that the anvil cloud feedback used in Sherwood et al. (2020) of  $-0.20 \text{ W m}^{-2} \text{ K}^{-1}$  to constrain the equilibrium climate sensitivity lies beyond the lower limit of our constraint and is likely too negative.

Motivated by the large uncertainty in the WCRP's estimate, recent studies also support a relatively neutral net feedback arising from changes in anvil cloud amount, with possibly more uncertainty from optical depth changes (McKim et al., 2024; Raghuraman et al., 2024; Sokol et al., 2024; Voigt, 2024). Thus, it has been suggested that the WCRP's negative anvil cloud feedback may actually arise from changes in optical depth as a result of cloud thinning, rather than decreases in amount (McKim et al., 2024; Sokol et al., 2024). Our findings of large-scale decreases in thick cloud is not inconsistent with a changing ratio of thick to thin cloud, and thus may constitute a (negative) optical depth feedback. We have not constrained the high-cloud optical depth feedback here due to weak historical monthly variability in  $R_r$  resulting in a small signal for the regression model to learn from (not shown; e.g. WK24), as well as potential non-linearity arising from phase changes which may not be sufficiently captured using linear methods. Observationally constraining the optical depth feedback is thus an important avenue for future work.

## 5. Summary

Cloud-controlling factor analysis has been used to constrain high-cloud feedback using CCFs previously linked to the life cycle of high clouds. We have constrained the net high-cloud amount feedback,  $\lambda_{\text{NET,AMT}}$ , through individual constraints on  $\lambda_{\text{LW,AMT}}$  and  $\lambda_{\text{SW,AMT}}$ . Importantly, we have shown that climate models underestimate LW and SW radiative feedbacks associated with reductions in high cloudiness with warming at local and global scales, likely due to poor representation of the thermodynamic controls of high-cloud amount within the climate models. This is reflected by the CCF responses to changes in static stability and surface temperature. Specifically, our observational constraint provides evidence for a stability iris mechanism that drives reductions in high-cloud amount in the deep tropics. We find that this mechanism is misrepresented by several climate models, contributing to weaker reductions in high-cloud amount within the GCM projections. Finally, our observational evidence suggests that global reductions in high cloudiness result in an approximately neutral cloud feedback—and not stabilizing as suggested in the assessment of Sherwood et al. (2020)—owing to compensating negative LW and positive SW feedbacks. While the multi-model mean high-cloud amount feedback is also neutral, several climate models achieve this result through cancellation of highly unlikely changes in high-cloud amount, according to our observational constraint.

## Data Availability Statement

All data used in this research is freely available. ERA5 meteorological reanalysis data are from the Copernicus Climate Change Service (Hersbach et al., 2023a, 2023b, 2023c). Combined MODIS Aqua–Terra data are freely available and downloaded with monthly resolution (NASA, 2022). CMIP5/6 (Eyring et al., 2016; Taylor et al., 2012) data are obtained from the UK Center for Environmental Data Analysis portal, CEDA (<https://esgf-node.llnl.gov>). Cloud radiative kernels are freely available at <https://github.com/mzelinka/cloud-radiative-kernels> (Zelinka, 2021).

## Acknowledgments

The authors would like to thank Mark Zelinka and Joel Norris for helpful discussions. We would also like to thank the two anonymous reviewers for their insightful feedback that has improved this research. This research has been supported by the UK Natural Environment Research Council, Grant NE/V012045/1 (SWK, PN, PC), NE/T006250/1 (PC) and the UK Government's Horizon Europe Funding Guarantee, Grant EP/Y036123/1 (PC). This research was carried out on the High Performance Computing Cluster supported by the Research and Specialist Computing Support service at the University of East Anglia and JASMIN, the UK's collaborative data analysis environment (<https://jasmin.ac.uk>). We acknowledge the World Climate Research Programme's Working Group on Coupled Modelling, which is responsible for CMIP, and we thank the climate modeling groups for producing and making available their model output. We also thank the Earth System Grid Federation (ESGF) for archiving the model output and providing access, and we thank the multiple funding agencies who support CMIP and ESGF.

## References

- Andersen, H., Cermak, J., Douglas, A., Myers, T. A., Nowack, P., Stier, P., et al. (2023). Sensitivities of cloud radiative effects to large-scale meteorology and aerosols from global observations. *Atmospheric Chemistry and Physics*, 23(18), 10775–10794. <https://doi.org/10.5194/acp-23-10775-2023>
- Andersen, H., Cermak, J., Zipfel, L., & Myers, T. A. (2022). Attribution of observed recent decrease in low clouds over the Northeastern Pacific to cloud-controlling factors. *Geophysical Research Letters*, 49(3), e2021GL096498. <https://doi.org/10.1029/2021GL096498>
- Beydoun, H., Caldwell, P. M., Hannah, W. M., & Donahue, A. S. (2021). Dissecting anvil cloud response to sea surface warming. *Geophysical Research Letters*, 48(15), e2021GL094049. <https://doi.org/10.1029/2021GL094049>
- Bony, S., Dufresne, J.-L., Le Treut, H., Morcrette, J.-J., & Senior, C. (2004). On dynamic and thermodynamic components of cloud changes. *Climate Dynamics*, 22(2), 71–86. <https://doi.org/10.1007/s00382-003-0369-6>
- Bony, S., Stevens, B., Coppin, D., Becker, T., Reed, K. A., Voigt, A., & Medeiros, B. (2016). Thermodynamic control of anvil cloud amount. *Proceedings of the National Academy of Sciences*, 113(32), 8927–8932. <https://doi.org/10.1073/pnas.1601472113>
- Bretherton, C. S., & Caldwell, P. M. (2020). Combining emergent constraints for climate sensitivity. *Journal of Climate*, 33(17), 7413–7430. <https://doi.org/10.1175/JCLI-D-19-0911.1>
- Byrne, M. P., & Schneider, T. (2018). Atmospheric dynamics feedback: Concept, simulations, and climate implications. *Journal of Climate*, 31(8), 3249–3264. <https://doi.org/10.1175/JCLI-D-17-0470.1>
- Ceppi, P., Brient, F., Zelinka, M. D., & Hartmann, D. L. (2017). Cloud feedback mechanisms and their representation in global climate models. *WIREs Climate Change*, 8(4), e465. <https://doi.org/10.1002/wcc.465>
- Ceppi, P., Myers, T. A., Nowack, P., Wall, C. J., & Zelinka, M. D. (2024). Implications of a pervasive climate model bias for low-cloud feedback. *Geophysical Research Letters*, 51(20), e2024GL110525. <https://doi.org/10.1029/2024GL110525>
- Ceppi, P., & Nowack, P. (2021). Observational evidence that cloud feedback amplifies global warming. *Proceedings of the National Academy of Sciences*, 118(30), e2026290118. <https://doi.org/10.1073/pnas.2026290118>
- Chen, T., Rossow, W. B., & Zhang, Y. (2000). Radiative effects of cloud-type variations. *Journal of Climate*, 13(1), 264–286. [https://doi.org/10.1175/1520-0442\(2000\)013<0264:REOCTV>2.0.CO;2](https://doi.org/10.1175/1520-0442(2000)013<0264:REOCTV>2.0.CO;2)
- Eyring, V., Bony, S., Meehl, G. A., Senior, C. A., Stevens, B., Stouffer, R. J., & Taylor, K. E. (2016). Overview of the Coupled Model Intercomparison Project Phase 6 (CMIP6) experimental design and organization. *Geoscientific Model Development*, 9(5), 1937–1958. <https://doi.org/10.5194/gmd-9-1937-2016>
- Fuchs, J., Cermak, J., & Andersen, H. (2018). Building a cloud in the southeast Atlantic: Understanding low-cloud controls based on satellite observations with machine learning. *Atmospheric Chemistry and Physics*, 18(22), 16537–16552. <https://doi.org/10.5194/acp-18-16537-2018>
- Gasparini, B., Sullivan, S. C., Sokol, A. B., Kärcher, B., Jensen, E., & Hartmann, D. L. (2023). Opinion: Tropical cirrus — From micro-scale processes to climate-scale impacts (preprint). Clouds and precipitation/atmospheric modelling and data analysis/troposphere. *Physics*. <https://doi.org/10.5194/egusphere-2023-1214>
- Gregory, J. M., Ingram, W. J., Palmer, M. A., Jones, G. S., Stott, P. A., Thorpe, R. B., et al. (2004). A new method for diagnosing radiative forcing and climate sensitivity. *Geophysical Research Letters*, 31(3). <https://doi.org/10.1029/2003GL018747>
- Hartmann, D. L., & Larson, K. (2002). An important constraint on tropical cloud - Climate feedback. *Geophysical Research Letters*, 29(20), 1–12. <https://doi.org/10.1029/2002GL015835>

- Hersbach, H., Bell, B., Berrisford, P., Biavati, G., Horányi, A., Muñoz Sabater, J., et al. (2023a). ERA5 hourly data on pressure levels from 1940 to present. *Copernicus Climate Change Service (C3S) Climate Data Store (CDS)*. [dataset]. <https://doi.org/10.24381/cds.bd0915c6>
- Hersbach, H., Bell, B., Berrisford, P., Biavati, G., Horányi, A., Muñoz Sabater, J., et al. (2023b). ERA5 monthly averaged data on pressure levels from 1940 to present. *Copernicus Climate Change Service (C3S) Climate Data Store (CDS)*. [dataset]. <https://doi.org/10.24381/cds.bd0915c6>
- Hersbach, H., Bell, B., Berrisford, P., Biavati, G., Horányi, A., Muñoz Sabater, J., et al. (2023c). ERA5 monthly averaged data on single levels from 1940 to present. *Dataset. Copernicus Climate Change Service (C3S) Climate Data Store (CDS)*. [dataset]. <https://doi.org/10.24381/cds.f17050d7>
- Klein, S. A., Hall, A., Norris, J. R., & Pincus, R. (2017). Low-cloud feedbacks from cloud-controlling factors: A review. *Surveys in Geophysics*, 38(6), 1307–1329. <https://doi.org/10.1007/s10712-017-9433-3>
- McFarquhar, G. M., Heymsfield, A. J., Spinhirne, J., & Hart, B. (2000). Thin and subvisual tropopause tropical cirrus: Observations and radiative impacts. *Journal of the Atmospheric Sciences*, 57(12), 1841–1853. [https://doi.org/10.1175/1520-0469\(2000\)057<1841:TASTTC>2.0.CO;2](https://doi.org/10.1175/1520-0469(2000)057<1841:TASTTC>2.0.CO;2)
- McKim, B., Bony, S., & Dufresne, J.-L. (2024). Weak anvil cloud area feedback suggested by physical and observational constraints. *Nature Geoscience*, 17(5), 1–6. <https://doi.org/10.1038/s41561-024-01414-4>
- Myers, T. A., & Norris, J. R. (2016). Reducing the uncertainty in subtropical cloud feedback. *Geophysical Research Letters*, 43(5), 2144–2148. <https://doi.org/10.1002/2015GL067416>
- Myers, T. A., Scott, R. C., Zelinka, M. D., Klein, S. A., Norris, J. R., & Caldwell, P. M. (2021). Observational constraints on low cloud feedback reduce uncertainty of climate sensitivity. *Nature Climate Change*, 11(6), 501–507. <https://doi.org/10.1038/s41558-021-01039-0>
- NASA. (2022). Modis (aqua/terra) cloud properties level 3 monthly, 1 x 1 degree grid. [dataset]. [https://doi.org/10.5067/MODIS/MCD06COSP\\_M3\\_MODIS.062](https://doi.org/10.5067/MODIS/MCD06COSP_M3_MODIS.062)
- Norris, J. R., & Evan, A. T. (2015). Empirical removal of artifacts from the ISCCP and PATMOS-x satellite cloud records. *Journal of Atmospheric and Oceanic Technology*, 32(4), 691–702. <https://doi.org/10.1175/JTECH-D-14-00058.1>
- Nowack, P., Braesicke, P., Luke Abraham, N., & Pyle, J. A. (2017). On the role of ozone feedback in the ENSO amplitude response under global warming. *Geophysical Research Letters*, 44(8), 3858–3866. <https://doi.org/10.1002/2016GL072418>
- Nowack, P., Ceppi, P., Davis, S. M., Chiodo, G., Ball, W., Diallo, M. A., et al. (2023). Response of stratospheric water vapour to warming constrained by satellite observations. *Nature Geoscience*, 16(7), 577–583. <https://doi.org/10.1038/s41561-023-01183-6>
- Nowack, P., Luke Abraham, N., Maycock, A. C., Braesicke, P., Gregory, J. M., Joshi, M. M., et al. (2015). A large ozone-circulation feedback and its implications for global warming assessments. *Nature Climate Change*, 5(1), 41–45. <https://doi.org/10.1038/nclimate2451>
- Nowack, P., & Watson-Parris, D. (2024). Opinion: Why all emergent constraints are wrong but some are useful - A machine learning perspective. *EGUSphere*, 1–28. <https://doi.org/10.5194/egusphere-2024-1636>
- Pincus, R., Hubanks, P. A., Platnick, S., Meyer, K., Holz, R. E., Botambekov, D., & Wall, C. J. (2023). Updated observations of clouds by MODIS for global model assessment. *Earth System Science Data*, 15(6), 2483–2497. <https://doi.org/10.5194/essd-15-2483-2023>
- Qu, X., Hall, A., Klein, S. A., & Caldwell, P. M. (2014). On the spread of changes in marine low cloud cover in climate model simulations of the 21st century. *Climate Dynamics*, 42(9), 2603–2626. <https://doi.org/10.1007/s00382-013-1945-z>
- Qu, X., Hall, A., Klein, S. A., & DeAngelis, A. M. (2015). Positive tropical marine low-cloud cover feedback inferred from cloud-controlling factors. *Geophysical Research Letters*, 42(18), 7767–7775. <https://doi.org/10.1002/2015GL065627>
- Rädel, G., Mauritsen, T., Stevens, B., Dommengat, D., Matei, D., Bellomo, K., & Clement, A. (2016). Amplification of El Niño by cloud longwave coupling to atmospheric circulation. *Nature Geoscience*, 9(2), 106–110. <https://doi.org/10.1038/ngeo2630>
- Raghruman, S. P., Medeiros, B., & Gettelman, A. (2024). Observational quantification of tropical high cloud changes and feedbacks. *Journal of Geophysical Research: Atmospheres*, 129(7), e2023JD039364. <https://doi.org/10.1029/2023JD039364>
- Saint-Lu, M., Bony, S., & Dufresne, J.-L. (2020). Observational evidence for a stability Iris effect in the tropics. *Geophysical Research Letters*, 47(14), e2020GL089059. <https://doi.org/10.1029/2020GL089059>
- Saint-Lu, M., Bony, S., & Dufresne, J.-L. (2022). Clear-sky control of anvils in response to increased CO<sub>2</sub> or surface warming or volcanic eruptions. *npj Climate and Atmospheric Science*, 5(1), 1–8. <https://doi.org/10.1038/s41612-022-00304-z>
- Scott, R. C., Myers, T. A., Norris, J. R., Zelinka, M. D., Klein, S. A., Sun, M., & Doelling, D. R. (2020). Observed sensitivity of low-cloud radiative effects to meteorological perturbations over the global oceans. *Journal of Climate*, 33(18), 7717–7734. <https://doi.org/10.1175/JCLI-D-19-1028.1>
- Sherwood, S. C., Bony, S., & Dufresne, J.-L. (2014). Spread in model climate sensitivity traced to atmospheric convective mixing. *Nature*, 505(7481), 37–42. <https://doi.org/10.1038/nature12829>
- Sherwood, S. C., Webb, M. J., Annan, J. D., Armour, K. C., Forster, P. M., Hargreaves, J. C., et al. (2020). An assessment of Earth's climate sensitivity using multiple lines of evidence. *Reviews of Geophysics*, 58(4), e2019RG000678. <https://doi.org/10.1029/2019RG000678>
- Sokol, A. B., Wall, C. J., & Hartmann, D. L. (2024). Greater climate sensitivity implied by anvil cloud thinning. *Nature Geoscience*, 17(5), 398–403. <https://doi.org/10.1038/s41561-024-01420-6>
- Taylor, K. E., Stouffer, R. J., & Meehl, G. A. (2012). An overview of CMIP5 and the experiment design. *Bulletin of the American Meteorological Society*, 93(4), 485–498. <https://doi.org/10.1175/bams-d-11-00094.1>
- Voigt, A. (2024). High clouds and higher sensitivity. *Nature Geoscience*, 17(5), 370–371. <https://doi.org/10.1038/s41561-024-01438-w>
- Webb, M. J., Lambert, F. H., & Gregory, J. M. (2013). Origins of differences in climate sensitivity, forcing and feedback in climate models. *Climate Dynamics*, 40(3), 677–707. <https://doi.org/10.1007/s00382-012-1336-x>
- Williams, I. N., & Pierrehumbert, R. T. (2017). Observational evidence against strongly stabilizing tropical cloud feedbacks. *Geophysical Research Letters*, 44(3), 1503–1510. <https://doi.org/10.1002/2016GL072202>
- Wills, R. C., Dong, Y., Proistosescu, C., Armour, K. C., & Battisti, D. S. (2022). Systematic climate model biases in the large-scale patterns of recent sea-surface temperature and sea-level pressure change. *Geophysical Research Letters*, 49(17). <https://doi.org/10.1029/2022GL100011>
- Wilson Kemsley, S., Ceppi, P., Andersen, H., Cermak, J., Stier, P., & Nowack, P. (2024). A systematic evaluation of high-cloud controlling factors. *Atmospheric Chemistry and Physics*, 24(14), 8295–8316. <https://doi.org/10.5194/acp-24-8295-2024>
- Wodzicki, K. R., & Rapp, A. D. (2022). More intense, organized deep convection with shrinking tropical ascent regions. *Geophysical Research Letters*, 49(15), e2022GL098615. <https://doi.org/10.1029/2022GL098615>
- Wyant, M. C., Bretherton, C. S., & Blossey, P. N. (2009). Subtropical low cloud response to a warmer climate in a superparameterized climate model. Part I: Regime sorting and physical mechanisms. *Journal of Advances in Modeling Earth Systems*, 1(3). <https://doi.org/10.3894/JAMES.2009.1.7>
- Zelinka, M. D. (2021). Mzelinka/cloud-radiative-kernels: Sep 17, 2021 release [Dataset]. <https://doi.org/10.5281/zenodo.5514137>
- Zelinka, M. D., Chao, L.-W., Myers, T., Qin, Y., & Klein, S. (2024). Technical note: Recommendations for diagnosing cloud feedbacks and rapid cloud adjustments using cloud radiative kernels. *EGUSphere*, 1–27. <https://doi.org/10.5194/egusphere-2024-2782>

- Zelinka, M. D., & Hartmann, D. L. (2010). Why is longwave cloud feedback positive? *Journal of Geophysical Research*, *115*(D16), D16117. <https://doi.org/10.1029/2010JD013817>
- Zelinka, M. D., & Hartmann, D. L. (2011). The observed sensitivity of high clouds to mean surface temperature anomalies in the tropics. *Journal of Geophysical Research*, *116*(D23). <https://doi.org/10.1029/2011JD016459>
- Zelinka, M. D., Klein, S. A., & Hartmann, D. L. (2012a). Computing and partitioning cloud feedbacks using cloud property histograms. Part I: Cloud radiative kernels. *Journal of Climate*, *25*(11), 3715–3735. <https://doi.org/10.1175/JCLI-D-11-00248.1>
- Zelinka, M. D., Klein, S. A., & Hartmann, D. L. (2012b). Computing and partitioning cloud feedbacks using cloud property histograms. Part II: Attribution to changes in cloud amount, altitude, and optical depth. *Journal of Climate*, *25*(11), 3736–3754. <https://doi.org/10.1175/JCLI-D-11-00249.1>
- Zelinka, M. D., Klein, S. A., Qin, Y., & Myers, T. A. (2022). Evaluating climate models' cloud feedbacks against expert judgment. *Journal of Geophysical Research: Atmospheres*, *127*(2), e2021JD035198. <https://doi.org/10.1029/2021JD035198>
- Zelinka, M. D., Myers, T. A., McCoy, D. T., Po-Chedley, S., Caldwell, P. M., Ceppi, P., et al. (2020). Causes of higher climate sensitivity in CMIP6 models. *Geophysical Research Letters*, *47*(1), e2019GL085782. <https://doi.org/10.1029/2019GL085782>
- Zelinka, M. D., Zhou, C., & Klein, S. A. (2016). Insights from a refined decomposition of cloud feedbacks. *Geophysical Research Letters*, *43*(17), 9259–9269. <https://doi.org/10.1002/2016GL069917>

## References From the Supporting Information

- Eaton, M. (1983). *Multivariate statistics: A vector space approach*. Institute of Mathematical Statistics.
- Pincus, R., Platnick, S., Ackerman, S. A., Hemler, R. S., & Patrick Hofmann, R. J. (2012). Reconciling simulated and observed views of clouds: MODIS, ISCCP, and the limits of instrument simulators. *Journal of Climate*, *25*(13), 4699–4720. <https://doi.org/10.1175/JCLI-D-11-00267.1>
- Reichler, T., Dameris, M., & Sausen, R. (2003). Determining the tropopause height from gridded data. *Geophysical Research Letters*, *30*(20). <https://doi.org/10.1029/2003GL018240>